Effect of C ion irradiation on AlGaAs/InGaAs HEMT

H. L. Wang[a], S. X. Sun[b,*] , H. Y. Mei[b,c], Y. T. Gao[b]
[a]*School of Material Science and Engineering, Zhengzhou University of Aeronautics, Zhengzhou 450015, China*
[b]*School of Electronic Information, Huanghuai University, Zhumadian 463000, China*
[c]*Key Laboratory of Functional Materials and Devices for Informatics of Anhui Educational Institutions, Fuyang Normal University, Fuyang, 236037*

In this paper, the damage caused by C ion irradiation on AlGaAs/InGaAs HEMT was investigated. The projection ranges of C ions with varying energies in AlGaAs and InGaAs materials were calculated using Monte Carlo simulation. Additionally, simulations were conducted to study the radiation-induced damage caused by 50 keV, 70 keV, and 100 keV C ions incident on the basic structure of the AlGaAs/InGaAs heterojunction.The results showed that when using 70 keV energy for C ions, a higher number of vacancy defects were generated. Based on these findings, the influence of defects introduced by different irradiation doses of 70 keV C ions on the DC and RF characteristics of the device was analyzed.

(Received May 30, 2023; Accepted September 1, 2023)

Keywords: AlGaAs/InGaAs HEMT, C ion irradiation, Vacancy defects, DC and RF characteristics

1. Introduction

In recent years, the utilization of microelectronic systems in key fields such as satellite radar, astronomical observation, and space communication has significantly increased due to the advancement of space exploration activities [1-3]. Integrated circuits play a crucial role in microelectronic systems, with semiconductor devices serving as the core components that determine their performance [4]. Among these devices, High Electron Mobility Transistors (HEMTs) based on AlGaAs/InGaAs have demonstrated exceptional advantages and immense potential for applications requiring high frequencies, low noise, and high power capabilities [5-7].

However, electronic devices operating in space are subjected to an extremely complex radiation environment consisting of solar wind, galactic cosmic rays, and radiation belts [8]. Prolonged exposure to ionizing radiation can result in functional degradation and even failure of device performance [9-11]. Therefore, understanding the influence of space radiation on

* Corresponding author: sunshuxianga@126.com

https://doi.org/10.15251/JOR.2023.195.483

semiconductor devices is crucial, and investigating the impact of space particles on these devices has become imperative [12]. Although there have been numerous studies conducted by research teams worldwide on the effects of particle irradiation on HEMTs, most of the research has focused on the effects of protons, electrons, and neutrons [13], while the effects of heavy ions on devices remain to be thoroughly investigated. Given that carbon ion (C ion) constitute a significant portion of heavy ions in the space radiation environment, this paper aims to investigate the damage caused by C ion irradiation on AlGaAs/InGaAs HEMTs using SRIM software. The relationship between vacancy defects and the electrical parameters of the devices is established to provide a theoretical foundation for the development of radiation-hardened devices.

2. Simulations

The structure of the AlGaAs/GaAs HEMT devices is illustrated in Table 1. Starting from the bottom, the device comprises a 1.5 μm GaAs substrate, a 10 nm $In_{0.25}Ga_{0.75}As$ channel layer, a 34.5 nm $Al_{0.3}Ga_{0.7}As$ isolation layer, a 30 nm GaAs cap layer, and a 50 nm Si_3N_4 passivation layer. The inclusion of InGaAs, with its narrower band gap compared to AlGaAs and GaAs, leads to the formation of a two-dimensional electron gas (2DEG). This introduces an additional layer of constraints on conventional HEMTs.The presence of the 2DEG contributes to a reduction in output conductance and an enhancement in power conversion efficiency when compared to traditional HEMTs.

Table 1. Structure of AlGaAs/InGaAs HEMT.

Material	Thickness
Si_3N_4	50 nm
GaAs	30 nm
$Al_{0.3}Ga_{0.7}As$	34.5 nm
$In_{0.25}Ga_{0.75}As$	10 nm
GaAs	1.5 um

The SRIM software is widely recognized and utilized internationally as a program based on the Monte Carlo method[14,15]. It calculates parameters such as incident incidence, energy transfer, and defect damage caused by charged particles in target materials. In this paper, the simulation of radiation damage zones and the underlying damage mechanisms in devices resulting from low-energy C ions is conducted using SRIM. To ensure efficient simulation speed and minimize errors, a total of 10^5 ions are utilized in this study. The threshold displacement energy for In, Ga, As and Al were set as 6.7 eV, 10 eV, 10 eV and 25 eV[16], respectively. The “Detailed Calculation with full Damage Cascades” mode was selected.

3. Results and discussion

3.1. Irradiation damage of $Al_{0.3}Ga_{0.7}As$ and $In_{0.25}Ga_{0.75}As$ materials by C ions with different energies

The study focuses on examining the microscopic interaction between C ions of different energies and materials. The average projection range and termination position of incident ions in the target material directly reflect the extent of radiation damage in the materials. Hence, the projection range of C ions with varying energies in $Al_{0.3}Ga_{0.7}As$ and $In_{0.25}Ga_{0.75}As$ materials was initially calculated. The obtained results were further subjected to linear regression analysis, as depicted in Fig. 1. As observed in the Fig., the projection range increases as the ion energy rises within the range of 10 KeV to 1 MeV, exhibiting an approximately linear relationship.

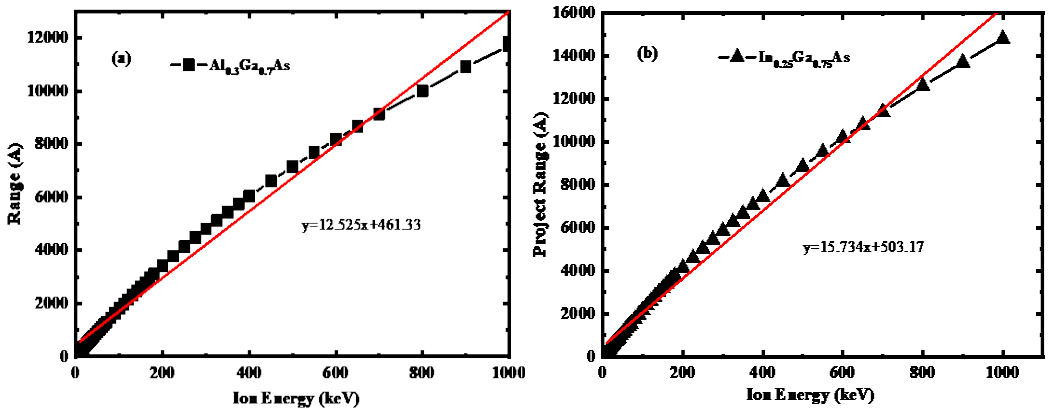

Fig. 1. Projection of C ions with different energies in the material, (a) $Al_{0.3}Ga_{0.7}As$; (b) $In_{0.25}Ga_{0.75}As$.

Fig. 2 presents the final stopping position of a 100keV C ion within the target material. It illustrates the discrete distribution of the incident ions within the material. Fig. 3 provides a three-dimensional representation of the C ion distribution within the target, allowing for a more intuitive visualization of the transverse and longitudinal distributions of the incident ions. Both Fig. 2 and Fig. 3 highlight that the final distribution of the incident ions is not solely confined to the initial direction of incidence. This indicates that during collisions with target atoms, incident ions are scattered in multiple directions, leading to cascade damage within the material. Consequently, this cascade effect increases the longitudinal damage distribution within the material or device.

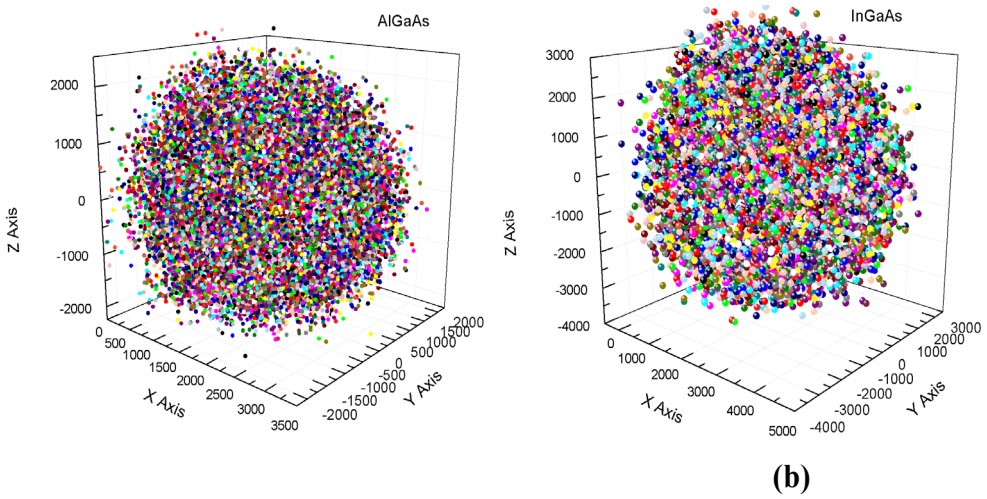

Fig. 2. Dispersion distribution of 100keV C ions in different targets, (a) $Al_{0.3}Ga_{0.7}As$; (b) $In_{0.25}Ga_{0.75}As$.

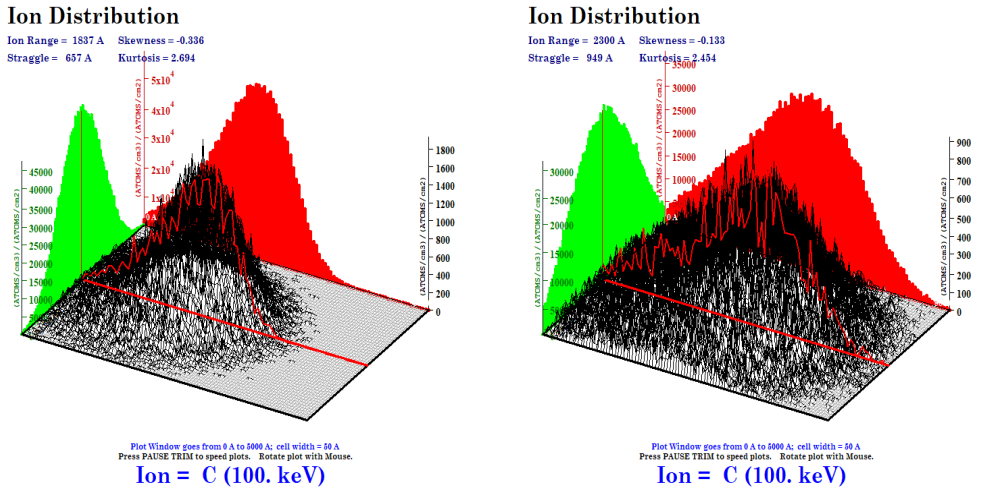

Fig. 3. Three-dimensional distribution of C ions at 100keV in different targets, (a) $Al_{0.3}Ga_{0.7}As$; (b) $In_{0.25}Ga_{0.75}As$.

The deceleration and energy loss experienced by incident ions primarily result from the interaction between the incident ions and the external electrons. The stopping power, denoted by the energy loss of the incident ion per unit path length (-dE/dX), characterizes the ability of the target nucleus and electrons to decelerate the incident ions. The electron stopping power and nuclear stopping power of $Al_{0.3}Ga_{0.7}As$ and $In_{0.25}Ga_{0.75}As$ are depicted in Fig. 4.From the Fig., it is evident that the electron stopping power increases with the energy of the incident ions, whereas the nuclear stopping power decreases with increasing ion energy. Furthermore, the electron stopping power significantly exceeds the nuclear stopping power.

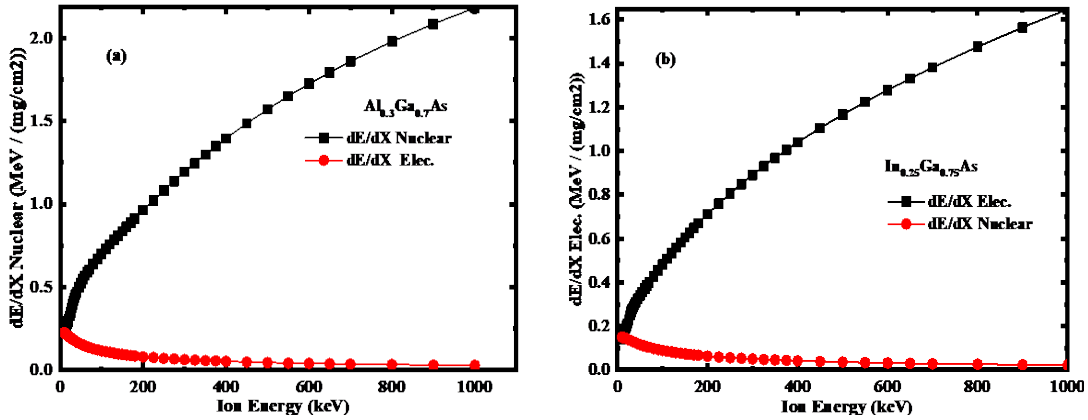

Fig. 4. Electron stopping power and nuclear stopping power of (a) $Al_{0.3}Ga_{0.7}As$ and (b) $In_{0.25}Ga_{0.75}As$.

3.2. Irradiation damage of AlGaAs/InGaAs HEMTs by C ion

The ionization damage in the device generates electron-hole pairs, which can recombine rapidly and do not have a permanent impact on the device. High-energy ions tend to penetrate through the device, while low-energy ions are more likely to remain within it. As a result, it is crucial to prioritize the investigation of radiation damage caused by low-energy ions in the device. Furthermore, particular attention should be given to defects at the heterojunction interface since they have the most significant impact on the device's performance. Specifically, defects in the barrier layer and channel layer of the device should be the focus of attention and analysis. Therefore, the device structure in Table 1 is adopted for simulation, and the vacancies induced by different energy C ions is calculated, as shown in Fig. 5.

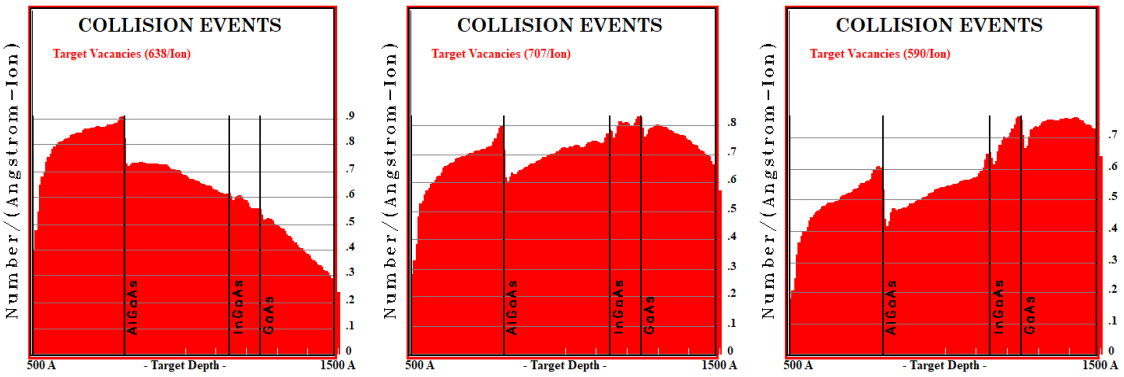

(a) *(b)* *(c)*

Fig. 5. The number of vacancies generated by C ions with different energies on both sides of the heterojunction, (a)50 keV; (b) 70 keV; (c) 100 keV.

As shown in Fig. 5, when the energy of the incident C ion is 50 keV, the generated vacancies are measured at 638 vacancies per Angstrom-Ion. When the ion energy increases to 70 keV, the number of vacancies rises to 707 vacancies per Angstrom-Ion. However, with a further

increase in ion energy to 100 keV, the number of vacancies decreases to 590 vacancies per Angstrom-Ion. This observation indicates that the vacancy generation initially increases and then decreases as the incident ion energy is raised. It is noteworthy that around 70 keV, the irradiation damage in the barrier layer and channel layer of the device is most severe, resulting in the highest number of generated vacancy defects. Fig. 6 displays the types of vacancies induced by 70 keV C ions on both sides of the AlGaAs/InGaAs heterojunction. The analysis reveals a significantly higher number of As and Ga vacancies in the AlGaAs barrier layer compared to the InGaAs channel layer. Moreover, the number of In vacancies exceeds that of Ga and As vacancies. This discrepancy can be attributed to the smaller displacement threshold energy of In atoms relative to As and Ga atoms, and notably smaller than that of Al atoms. The lower the displacement threshold energy of atoms, the higher the likelihood of their ejection from the lattice, leading to the formation of vacancy defects. The variation of vacancy with depth is shown in Fig. 7. It can be seen that the atomic vacancy generated on both sides of the heterojunction changes little with depth.

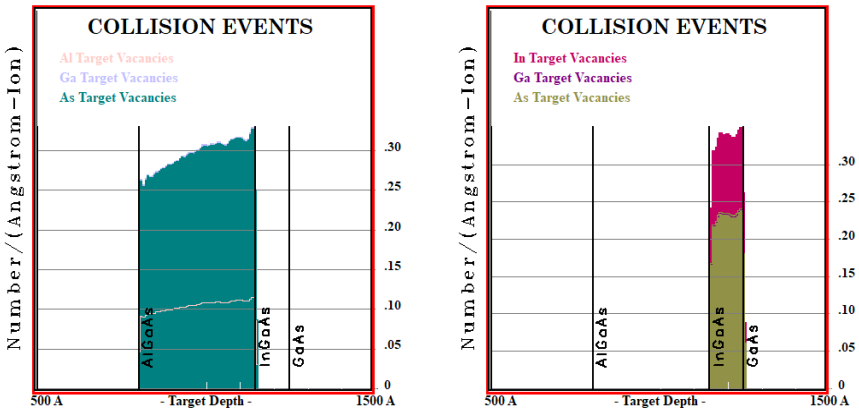

(a) *(b)*

Fig. 6. Number of vacancies generated by C ions at 70keV on both sides of the heterojunction, (a) $Al_{0.3}Ga_{0.7}As$ and (b) $In_{0.25}Ga_{0.75}As$.

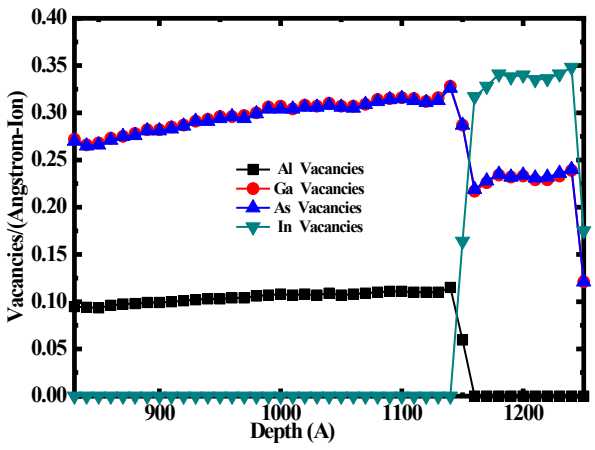

Fig. 7. Vacancy changes with target depth.

Fig. 8 depicts the relationship between vacancy concentration and ion dose when incident 70 keV C ions are utilized. It is evident from the Fig. that the concentration of various vacancies on both sides of the heterojunction displays a linear relationship with the increasing dose of C ion implantation. This observation indicates that a higher dose of ion implantation results in the formation of a greater number of vacancy defects.

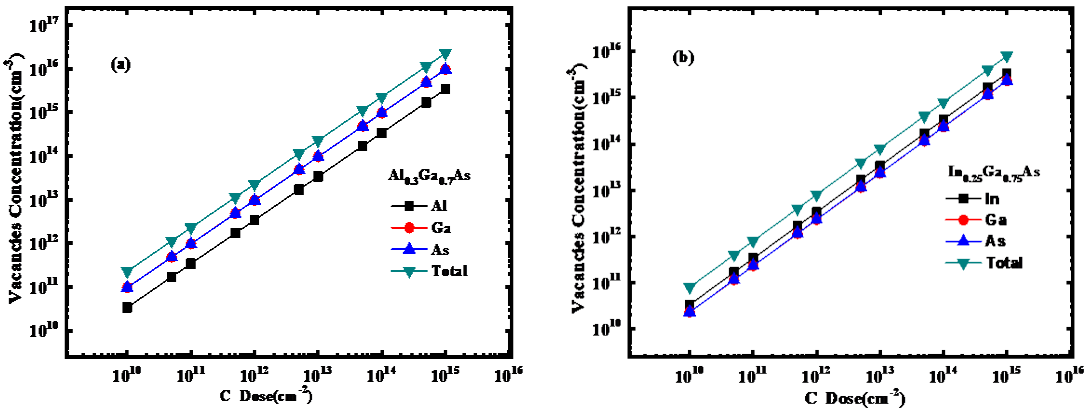

Fig. 8. Variation of vacancy concentration with incident ion dose, (a) $Al_{0.3}Ga_{0.7}As$ and (b) $In_{0.25}Ga_{0.75}As$.

To verify the impact of irradiation-induced vacancies on the device, the vacancy concentrations induced by 70 keV with the ion doses of 5×10^{16} and 1×10^{17} were introduced into the device model established using TCAD software. The variation of device characteristics with the ion injection amount was subsequently calculated and depicted in Fig. 9. As observed in the Fig. 9, the saturated drain current and transconductance gradually decrease as the ion dose increases. This decline can be attributed to the generation of more defects with increasing dose. The increased defects capture more charge carriers, resulting in a more pronounced degradation of device performance.

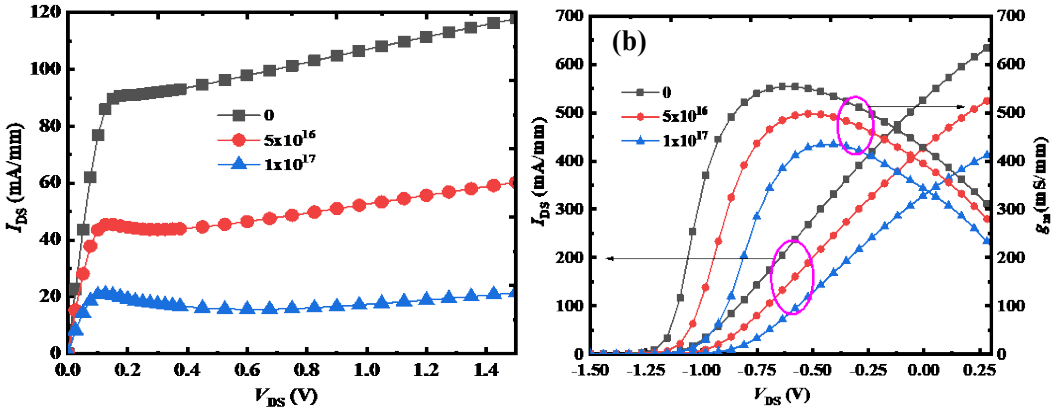

Fig. 9. Variation of (a) output characteristics and (b) transfer characteristics with incident ion dose.

4. Conclusions

In summary, the effects of C ion irradiation on AlGaAs/InGaAs HEMTs were investigated through numerical simulation. The results showed that the projection range increases as the ion energy rises within the range of 10 KeV to 1 MeV, exhibiting an approximately linear relationship. Incident ions are scattered in multiple directions, leading to cascade damage within the material. It is noteworthy that around 70 keV, the irradiation damage in the barrier layer and channel layer of the device is most severe, resulting in the highest number of generated vacancy defects. Moreover, the saturated drain current and transconductance gradually decrease as the ion dose increases.

Acknowledgements

This work was supported by the National Natural Science Foundation of China (Grant No. 62204094), China Postdoctoral Science Foundation (Grant No. 2021M700685), Henan Provincial Science and Technology Research Project (Grant No. 232102210173, 232102311204), Joint Fund of Henan Province Science and Technology Research and Development Plan, Open Project of Provincial and Ministerial Scientific Research Platform, Fuyang Normal University (Grant No. FSKFKT015D), Major science and technology project of Zhumadian City of 2022 (Grant No. ZMDSZDZX2022004), .

References

[1] N. Wu, Z. H. Xing, S. J. Li, L. Luo, F. Y. Zeng, G. Q. Li, Semicond. Sci. Technol. 38, 063002 (2023); https://doi.org/10.1088/1361-6641/acca9d

[2] J. Y. Wang, J. Liu, J. Wang, Z. X. Zhao, Micromachines 14, 1023 (2023); https://doi.org/10.3390/mi14051023

[3] M. A. Alim, A. Jarndal, C. Gaquiere, Gi. Crup, Journal of Materials Science: Materials in Electronics 34, 892 (2023); https://doi.org/10.1007/s10854-023-10176-5

[4] J. Ajayan, D. Nirmal, Superlattices and Microstructures 86, 1-19 (2015); https://doi.org/10.1016/j.spmi.2015.06.048

[5] J. Ajayan, D. Nirmal, P. Mohankumar, Dheena Kuriyan, A.S. Augustine Fletcher, L. Arivazhagan, B. Santhosh Kumar, Microelectronics Journal 92, 104604 (2019); https://doi.org/10.1016/j.mejo.2019.104604

[6] X. Yan,H. R. Luo, J. Y. Zhang, H. Zhang, Y. X. Guo, IEEE Transactions on Circuits and Systems-II: Express Briefs 69(12), 4659- 4663 (2022); https://doi.org/10.1109/TCSII.2022.3196817

[7] S. H. Shin, J. P. Shim, H. Jang, J. H. Jang, Micromachines 14, 56 (2023); https://doi.org/10.3390/mi14040796

[8] Y. H. Zhong, B. Yang, M. M Chang, P. Ding, L. H Ma, M. K. Li, Z. Y. Duan, J. Yang, Z. Jin, Z. C. Wei, Chinese Physics B 29(3), 038502 (2020); https://doi.org/10.1088/1674-1056/ab6962

[9] J. G. Kim, E. Kim, D. S. Kim, C. Cho, J. H. Lee, IEEE Journal of the Electron Devices Society,

10, 19-22 (2022); https://doi.org/10.1109/JEDS.2021.3128191

[10] P. Wan, J. Yang, T. Ying, G. Lv, L. Lv, S. Dong, Lei D., X. Yu, Z. Zhen, W. Li, X. Li, IEEE Transactions on Nuclear Science, 68(6), 1265-1271 (2021); https://doi.org/10.1109/TNS.2021.3074391

[11] J. J. Tang, G. P. Liu, B. Y. Mao, S. Ali, G. J. Zhao, J. H. Yang, Physics Letters A 410, 127527 (2021); https://doi.org/10.1016/j.physleta.2021.127527

[12] S. J. Pearton, F. Ren, E. Patrick, M. E. Law, Alexander Y. Polyakov, ECS Journal of Solid State Science and Technology 5 (2), Q35-Q60 (2016); https://doi.org/10.1149/2.0251602jss

[13] S. J. Pearton, A. Aitkaliyeva, M. Xian, F. Ren, A. Khachatrian, A. Ildefonso, Z. Islam, M. A. J. Rase, A. Haque, A.Y. Polyakov, J. Kim, ECS Journal of Solid State Science and Technology 10, 055008 (2021); https://doi.org/10.1149/2162-8777/abfc23

[14] S. X. Sun, Y. Z. Wu, H. Y. Mei, Digest Journal of Nanomaterials and Biostructures 18(2), 557-566 (2023); https://doi.org/10.15251/DJNB.2023.182.557

[15] H. Y. Mei, S. H. Zhao, Y. Z. Wu, P. Zhang, H. T. Wu, R. X. Yao, X. Y. Zheng, H. Wen, S. X. Sun, Digest Journal of Nanomaterials and Biostructures 17(2), 749-758 (2022).

[16] Xiao-Hong Zhao, Hong-Liang Lu, Yu-Ming Zhang, Yi-Men Zhang, Microelectronics Reliability 78 (2017) 156-160; https://doi.org/10.1016/j.microrel.2017.07.097